WATER RESOURCES RESEARCH, VOL. 30, NO. 12, PAGES 3357–3374, DECEMBER 1994

A comparison of Picard and Newton iteration in the numerical solution of multidimensional variably saturated flow problems

Claudio Paniconi
Centro di Ricerca, Sviluppo e Studi Superiori in Sardegna, Cagliari, Italy

Mario Putti
Dipartimento di Metodi e Modelli Matematici per le Scienze Applicate
Università di Padova, Padua, Italy

Abstract. Picard iteration is a widely used procedure for solving the nonlinear equation governing flow in variably saturated porous media. The method is simple to code and computationally cheap, but has been known to fail or converge slowly. The Newton method is more complex and expensive (on a per-iteration basis) than Picard, and as such has not received very much attention. Its robustness and higher rate of convergence, however, make it an attractive alternative to the Picard method, particularly for strongly nonlinear problems. In this paper the Picard and Newton schemes are implemented and compared in one-, two-, and three-dimensional finite element simulations involving both steady state and transient flow. The eight test cases presented highlight different aspects of the performance of the two iterative methods and the different factors that can affect their convergence and efficiency, including problem size, spatial and temporal discretization, initial solution estimates, convergence error norm, mass lumping, time weighting, conductivity and moisture content characteristics, boundary conditions, seepage faces, and the extent of fully saturated zones in the soil. Previous strategies for enhancing the performance of the Picard and Newton schemes are revisited, and new ones are suggested. The strategies include chord slope approximations for the derivatives of the characteristic equations, relaxing convergence requirements along seepage faces, dynamic time step control, nonlinear relaxation, and a mixed Picard-Newton approach. The tests show that the Picard or relaxed Picard schemes are often adequate for solving Richards' equation, but that in cases where these fail to converge or converge slowly, the Newton method should be used. The mixed Picard-Newton approach can effectively overcome the Newton scheme's sensitivity to initial solution estimates, while comparatively poor performance is reported for the various chord slope approximations. Finally, given the reliability and efficiency of current conjugate gradient–like methods for solving linear nonsymmetric systems, the only real drawback of using Newton rather than Picard iteration is the algebraic complexity and computational cost of assembling the derivative terms of the Jacobian matrix, and it is suggested that both methods can be effectively implemented and used in numerical models of Richards' equation.

1. Introduction

The governing equation for flow in partially saturated porous media, Richards' equation, contains nonlinearities arising from pressure head dependencies in soil moisture and hydraulic conductivity. For stability reasons an implicit time discretization, requiring evaluation of the nonlinear coefficients at the current time level, is normally used to solve the equation numerically. To linearize the resulting discrete system of equations, Newton or Picard iteration is commonly used, with the Picard scheme being the more popular of the two [*Frind and Verge*, 1978; *Hills et al.*, 1989; *Huyakorn et al.*, 1986; *Kuiper*, 1987; *Neuman*, 1973; *Ross*, 1990; *Stauffer*, 1982]. The Picard method, also known as successive approximation or "simple" iteration, enjoys great popularity because it is the most intuitive linearization of Richards' equation, is computationally inexpensive on a per-iteration basis, and preserves symmetry of the discrete system of equations. However, the method may diverge under certain conditions, as has been observed empirically [e.g., *Huyakorn et al.*, 1984; *Celia et al.*, 1990] and verified theoretically [*Aldama and Paniconi*, 1992]. The Newton scheme, also known as Newton-Raphson iteration, yields nonsymmetric system matrices and is more complex and expensive than Picard linearization, though it achieves a higher rate of convergence and can be more robust than Picard for certain types of problems. Use of the Newton scheme has been limited to one- and two-dimensional unsaturated flow models [*Brutsaert*, 1971; *Cooley*, 1983; *Faust*, 1985; *Huyakorn et al.*, 1984]. A detailed comparison of the Picard and Newton methods has been conducted for the transient one-dimensional Richards equation [*Paniconi et al.*, 1991], where it was shown that, in terms of CPU needed

Paper number 94WR02046.
0043-1397/94/94WR-02046$05.00

to attain a given level of solution accuracy, Newton iteration can be as or more efficient than Picard.

In this paper the previous evaluation of the Picard and Newton methods for the transient one-dimensional case is extended to steady state and transient simulations of one-, two-, and three-dimensional subsurface flow processes. Two- and three-dimensional simulations give rise to larger problems (of size $O(N^2)$ or $O(N^3)$ where N represents the number of unknowns across one dimension) and more complex dynamics (free surfaces, variable flow paths) and boundary conditions (seepage faces, multiple sources and sinks, spatially variable rainfall and evaporation inputs). These factors, along with the nature of the moisture content–pressure head and hydraulic conductivity–pressure head relationships, will have important effects on the performance of iterative schemes. Multidimensional simulations also introduce considerations which are negligible in the one-dimensional case, such as the efficiency of linear solvers for large, sparse, symmetric and nonsymmetric systems. In steady state simulations the corrective mechanism of dynamic time step adjustment is lost, which in the transient case can be used to improve an initial solution estimate, via a reduction in time step size, whenever convergence of a nonlinear iterative scheme is too slow or fails.

Several techniques have been proposed to enhance the performance of the Picard and Newton methods for cases where convergence troubles are encountered. These techniques, which include relaxation and chord slope differentiation, are implemented, along with a new mixed approach involving the use of Picard iteration to improve the initial solution estimate for the Newton scheme. The Newton and Picard schemes are compared under a variety of conditions via finite element simulation of eight test problems. The test problems illustrate the circumstances under which the two iterative schemes can be expected to perform poorly, and the results suggest avenues for more detailed analysis and for investigation of other approaches to solving the nonlinear flow equation.

2. Numerical Procedures

2.1. Governing Equation and Finite Element Models

The partial differential equation describing fluid flow in partially saturated porous media, Richards' equation, is obtained by combining Darcy's law with the continuity equation [*Philip*, 1969]. Expressing this equation with pressure head ψ as the dependent variable, t as time, and z as the vertical coordinate (positive upward) yields

$$\eta(\psi)\frac{\partial \psi}{\partial t} = \nabla \cdot (K_s K_r(\psi)\nabla(\psi + z)) \tag{1}$$

where $\eta(\psi)$ is the general storage term or overall storage coefficient and the hydraulic conductivity tensor is expressed as a product of the conductivity at saturation, K_s, and the relative conductivity, $K_r(\psi)$. Equation (1) is highly nonlinear due to pressure head dependencies in the storage and conductivity terms.

To solve (1) numerically, a finite element Galerkin discretization in space with linear basis functions is used. Triangular elements are used in the two-dimensional code, and either tetrahedral or hexahedral elements in three dimensions. With tetrahedra the nonlinear coefficients in the system integrals are evaluated at the element centroids, whereas with hexahedral elements order 2 Gaussian quadrature is used to evaluate the integrals. A λ-weighted finite difference scheme is used for time discretization ($\lambda = 0.5$, Crank-Nicolson; $\lambda = 1$, backward Euler). Details of the numerical procedures can be found in standard texts [e.g., *Ames*, 1977; *Huyakorn and Pinder*, 1983]. Discretization yields the system of nonlinear equations

$$\mathbf{f}(\Psi^{k+1}) \equiv \mathbf{A}(\Psi^{k+\lambda})\Psi^{k+\lambda} + \mathbf{F}(\Psi^{k+\lambda})\frac{\Psi^{k+1} - \Psi^{k}}{\Delta t^{k+1}} + \mathbf{b}(\Psi^{k+\lambda}) - \mathbf{q}(t^{k+\lambda}) = \mathbf{0} \tag{2}$$

where $\Psi^{k+\lambda} = \lambda\Psi^{k+1} + (1 - \lambda)\Psi^{k}$, Ψ is the vector of nodal pressure heads, superscript k denotes time step, $\mathbf{A}$ is the stiffness matrix, $\mathbf{F}$ is the storage or mass matrix, $\mathbf{b}$ contains the gravitational gradient component of (1), and $\mathbf{q}$ contains the specified Darcy flux boundary conditions.

The numerical models have the option of using either distributed or lumped mass matrices. The models can handle a variety of boundary conditions, including atmospheric inputs, seepage faces, and source/sink terms such as pumping wells. The handling of atmospheric (rainfall and evaporation) inputs is described by *Paniconi and Wood* [1993], while seepage faces are treated by a variant of the method described by *Cooley* [1983] and *Huyakorn et al.* [1986], where we have introduced two options controlled by the zero-one flags sf_1 and sf_{cvg}. If $sf_1 = 0$, updating of the seepage face exit point is performed by checking all nodes on a seepage face, while if $sf_1 = 1$, only the nodes directly above and below the exit point are checked. If $sf_{cvg} = 0$, convergence of the exit point is not a condition for convergence of the nonlinear iterative scheme, while if $sf_{cvg} = 1$, the exit point must converge in order to obtain overall solution convergence. Thus sf_1 and sf_{cvg} allow us to relax the convergence requirements along seepage faces, with $sf_1 = 0$, $sf_{cvg} = 1$ being the most stringent of the four possible combinations.

2.2. Linearization Techniques

2.2.1. Newton and Picard iteration. Applied to (2), the Newton scheme can be written as

$$\mathbf{f}'(\Psi^{k+1,(m)})\mathbf{h} = -\mathbf{f}(\Psi^{k+1,(m)}) \tag{3}$$

where $\mathbf{h} \equiv \Psi^{k+1,(m+1)} - \Psi^{k+1,(m)}$, superscript (m) is an iteration index, and

$$f'_{ij} = \lambda A_{ij} + \frac{1}{\Delta t^{k+1}}F_{ij} + \sum_s \frac{\partial A_{is}}{\partial \psi_j^{k+1}}\psi_s^{k+\lambda} + \frac{1}{\Delta t^{k+1}}\sum_s \frac{\partial F_{is}}{\partial \psi_j^{k+1}}(\psi_s^{k+1} - \psi_s^{k}) + \frac{\partial b_i}{\partial \psi_j^{k+1}} \tag{4}$$

is the ijth component of the Jacobian matrix $\mathbf{f}'(\Psi^{k+1})$.

The Picard scheme may be written as

$$\left[\lambda\mathbf{A}(\Psi^{k+\lambda,(m)}) + \frac{1}{\Delta t^{k+1}}\mathbf{F}(\Psi^{k+\lambda,(m)})\right]\mathbf{h} = -\mathbf{f}(\Psi^{k+1,(m)}) \tag{5}$$

Comparing (3) and (5), it is apparent that the Picard scheme can be viewed as an approximate Newton method. It can be shown that under suitable conditions the Newton scheme is quadratically convergent [*Stoer and Bulirsch*, 1980], while Picard converges only linearly. Another important difference between the two schemes is that Newton linearization generates a nonsymmetric system matrix, whereas Picard preserves the symmetry of the original discretization. This factor is important in assessing the relative efficiency of the two schemes, since different storage and linear solver algorithms can be used to exploit these structural differences. A final observation to make is that calculation of the three derivative terms in the Jacobian makes the Newton scheme more costly and algebraically complex than Picard. In our numerical tests the per-iteration CPU cost of the Newton method was found to be approximately twice that of the Picard method, independent of the dimensionality of the problem. A more detailed discussion of the Newton and Picard schemes applied to the unsaturated flow equation can be found in the work by *Paniconi et al.* [1991].

Time step sizes during a transient simulation are dynamically adjusted according to the convergence behavior of the nonlinear iteration scheme. A convergence tolerance tol is specified, along with a maximum number of iterations, maxit, permitted during any time step. The simulation begins with a time step size of Δt_0 and proceeds until time $T_{\max}$. The current time step size is increased by a factor of Δt_{mag} (to a maximum size of $\Delta t_{\max}$) if convergence is achieved in fewer than maxit_1 iterations, it is left unchanged if convergence required between maxit_1 and maxit_2 iterations, and it is decreased by a factor of Δt_{red} (to a minimum of $\Delta t_{\min}$) if convergence required more than maxit_2 iterations. If convergence is not achieved (maxit exceeded), the solution at the current time level is recomputed ("back stepping") using a reduced time step size (factor Δt_{red}, to a minimum of $\Delta t_{\min}$). For the first time step of a transient simulation, or for steady state problems, the initial conditions are used as the first solution estimate for the iterative procedure. For subsequent time steps of a transient simulation the pressure head solution from the previous step is used as the first estimate. Thus time step size has a direct effect on convergence behavior, via its influence on the quality of the initial solution estimate.

The infinity norm (l_∞) of the convergence error is used in the termination criterion for the nonlinear iterative methods; that is, convergence is achieved when $\|\Psi^{k+1,(m+1)} - \Psi^{k+1,(m)}\|_\infty \leq \text{tol}$ is satisfied. This represents a measure of absolute error, but it can also be used to measure relative (normalized) error by selecting tol to be a suitable multiple of some reference pressure head value [*Matthies and Strang*, 1979]. In test case 2S the behavior of the convergence error using the l_2 norm (the square root of the sum of squares of pressure head differences over all nodes) is examined in addition to the l_∞ norm, and the residual error ($\|\mathbf{f}(\Psi^{k+1,(m)})\|$) is also computed using the l_∞ and l_2 norms.

2.2.2. Relaxation and mixed Picard-Newton methods. Relaxation (or damping) has been suggested as a way of enhancing convergence of nonlinear iterative schemes, in particular when oscillations in $\mathbf{h}$ occur from one iteration to the next [*Cooley*, 1983]. Two different methods of calculating the relaxation parameter were implemented in our codes. The first is *Huyakorn et al.*'s [1986] adaptation of *Cooley*'s [1983] empirical scheme, where the relaxation parameter Ω is calculated at the end of each iteration as a function of the solution at the current and previous iterations. The current solution $\Psi^{k+1,(m+1)}$ is then updated (relaxed) to Ψ^* by the relationship $\Psi^* = \Omega\Psi^{k+1,(m+1)} + (1 - \Omega)\Psi^{k+1,(m)}$. In the second option, Ω is constant, and the relaxation step can be equivalently expressed by multiplying the right-hand sides of the Newton equation (3) or the Picard equation (5) by Ω [*Ababou et al.*, 1988].

In many of our test simulations we observed the Newton scheme to be quite sensitive to the initial solution estimate. With a poor initial estimate the Newton scheme can diverge, whereas when the estimate is good Newton converges very rapidly. Our observations also suggest that the Picard method does not generally diverge; poor Picard performance is more often manifested by low or zero average convergence rate. In order to exploit the best features of both methods, a mixed Picard-Newton approach was tested, based on the idea of using Picard iteration to improve the "initial" solution estimate for the Newton method. In this approach the Picard scheme is used for the first few iterations, until it has begun to converge steadily, and then the Newton scheme is used for the remaining iterations. In our implementation, once Picard iteration begins to converge, the switch to Newton is done after a specified reduction in convergence error has been achieved.

2.3. Linear Solvers

One of the main drawbacks of the Newton scheme used to be the inefficiency of linear solvers for large, sparse nonsymmetric systems. This is no longer the case, as currently available conjugate gradient–type algorithms for solving nonsymmetric systems have become increasingly reliable and efficient. In our tests we obtained best results using a biconjugate gradient stabilized algorithm, BICGSTAB, although we also tried a minimum residual algorithm, GRAMRB, a generalized conjugate residual method, GCRK, and the transpose-free quasi-minimal residual algorithm, TFQMR. All these schemes were used with incomplete Croute lower-upper (LU) decomposition as a preconditioner. Descriptions of the various algorithms can be found in the works by *Axelsson* [1980], *Pini et al.* [1989], *van der Vorst* [1992], and *Freund* [1993]. For the symmetric systems generated by Picard linearization we used the incomplete Cholesky conjugate gradient method, ICCG [*Kershaw*, 1978; *Gambolati and Perdon*, 1984]. In one of the smaller test cases, 1Ta, a tridiagonal direct solver was used for both the symmetric and nonsymmetric systems. For all the other test cases, where ICCG, BICGSTAB, or some other iterative solver was used, Table 1 gives the values used for the linear solver parameters tolcg (convergence tolerance) and maxitcg (maximum number of iterations allowed).

2.4. Characteristic Equations and Chord Slope Approximations

The nonlinear storage and conductivity terms in (1) can be modeled using various constitutive or characteristic relations describing the soil hydraulic properties. One of the simplest of these, useful for steady state simulations, is the exponential $K_r(\psi)$ relationship [*Pullan*, 1990]

$$K_r(\psi) = \exp(\alpha\psi) \tag{6}$$

where α is a constant.

Table 1. Description of the Test Cases

Test Case	Dimension	Steady State/ Transient	Domain Size	Grid Discretization	Number of Nodes	Number of Elements	Simulation Time (T_{max})	Time Discretization Parameters	Nonlinear Iteration Parameters	Linear Solver	Linear Solver Parameters
1S	1	steady state	L_z = 3; 7; 10; 20; 30 m	Δz = 0.01; 0.001 m	3001; 7001; 10,001; 20,001; 30,001	3000; 7000; 10,000; 20,000; 30,000			tol = 1e−12;* 1e−9 m, maxit = 1000, maxit_1 = 1000, maxit_2 = 1000	ICCG (symmetric), BICGSTAB (nonsymmetric)	tolcg = 1e−26, maxitcg = 1000
1Ta	1	transient	L_z = 10 m	Δz = 0.1 m	101	100	32 hours	Δt = 0.005; ⋯ ; 1.0 hour, Δt_{red} = 1, Δt_{mag} = 1	tol = 1e−3 m, maxit = 1000, maxit_1 = 1000, maxit_2 = 1000	tridiagonal	
2S	2	steady state	L_x = 100 m, L_z = 100 m	Δx = 10; 2 m, Δz = 10; 2 m	121; 2601	200; 5000 (triangles)			tol = 1e−6 m, maxit = 1500, maxit_1 = 1500, maxit_2 = 1500	ICCG (symmetric), BICGSTAB (nonsymmetric)	tolcg = 1e−12, maxitcg = 5000
2T	2	transient	L_x = 15 cm, L_z = 10 cm	Δx = 1; 0.25 cm, Δz = 1 cm	176; 671	300; 1200 (triangles)	5; 0.01; 0.005 days	Δt_0 = 1e−5; ⋯ ; 5e−1 day, Δt_{min} = 1e−6, Δt_{max} = 1e−5; 1.5, Δt_{red} = 0.6, Δt_{mag} = 1.3	tol = 1e−6 cm, maxit = 50; 500, maxit_1 = 10, maxit_2 = 30	ICCG (symmetric), BICGSTAB (nonsymmetric)	tolcg = 1e−12, maxitcg = 1000
3S	3	steady state	L_x = 1000 m, L_y = 400 m, L_z = 72 m	Δx = [30, 75] m, Δy = 50 m, Δz = [5, 15] m	2079	9600 (tetrahedra)			tol = 1e−6 m, maxit = 100, maxit_1 = 100, maxit_2 = 100	ICCG (symmetric), BICGSTAB (nonsymmetric)	tolcg = 1e−10, maxitcg = 1000
3Ta	3	transient	L_x = 1000 m, L_y = 400 m, L_z = 72 m	Δx = [30, 75] m, Δy = 50 m, Δz = [5, 15] m	2079	9600 (tetrahedra)	5000 days	Δt_0 = 2e−5 day, Δt_{min} = 1e−5, Δt_{max} = 100, Δt_{red} = 0.6, Δt_{mag} = 1.12	tol = 1e−6 m, maxit = 100, maxit_1 = 25, maxit_2 = 50	ICCG (symmetric), various (nonsymmetric)	tolcg = 1e−10, maxitcg = 1000
3Tb	3	transient	surface area = 0.24 km^2, L_z = 1 m	Δx = 30 m, Δy = 30 m, Δz = [0.002, 0.1] m	8164	6650 (hexahedra)	336; 30,000 hours	Δt_0 = 0.1; 1 hour, Δt_{min} = 1e−3, Δt_{max} = 12; 200, Δt_{red} = 0.6, Δt_{mag} = 1.15	tol = 5e−4; 5e−2 m, maxit = 50, maxit_1 = 12, maxit_2 = 30	ICCG (symmetric), GRAMRB (nonsymmetric)	tolcg = 1e−10, maxitcg = 1000
1Tb	1	transient	L_z = 1 m	Δz = 0.04; [0.002, 0.1]; 0.002 m	26; 26; 501	25; 25; 500	336 hours	Δt_0 = 0.1 hour, Δt_{min} = 1e−6, Δt_{max} = 12, Δt_{red} = 0.6, Δt_{mag} = 1.15	tol = 5e−4 m, maxit = 50, maxit_1 = 25, maxit_2 = 25	ICCG (symmetric), GRAMRB (nonsymmetric)	tolcg = 1e−10, maxitcg = 1000

*Read 1e−12 as 1×10^{-12}.

Table 2. Soil Characteristics and Boundary and Initial Conditions for the Test Cases

Test Case	Boundary Conditions (No-Flow Conditions on All Other Boundaries)	Initial Conditions/Solution Estimates	Characteristic Equations and Parameters	Saturated Conductivity and Air-Dry Pressure Head
1S	$\psi = 0$ at $z = 0$; $K(\psi)((\partial\psi/\partial z) + 1) = 0.01$ at $z = L_z$	$\psi(z) = -3z/L_z$; $\psi(z) = -z$ for $z \le 3$, $\psi(z) = -3$ for $z > 3$	equation (6): $\alpha = 1$	$K_s = 0.1$ m/h
1Ta	$\psi = 0$ at $z = 0$; $K(\psi)((\partial\psi/\partial z) + 1) = t/64$ at $z = L_z$	$\psi(z, 0) = -z$	equations (10) and (8): $\theta_r = 0.08$, $\theta_s = 0.45$, $S_s = 0.001$, $\psi_0 = -0.19105548$, $n = 3$, $\psi_s = -3$	$K_s = 5$ m/h
2S	$\psi = 100 - z$ at $x = 0$, $0 \le z \le 100$; $\psi = 20 - z$ at $x = 100$, $0 \le z \le 20$; seepage face at $x = 100$, $20 < z \le 100$	$\psi(x, z) = 100 - z$	equation (12): $\alpha = (0.1)^{1/4}$, $\psi_a = 0$, $\gamma = 1$, $\beta = 1; 2; 4$, $n = 2; 4$ equation (8): $n = 1.5; 3; 5$, $\psi_s = -3; -20$	$K_s = 0.01$ m/h
2T	$\psi = 6 - z$ at $x = 0$, $6 \le z \le 10$; $\psi = -90$ at $x = 15$, $0 \le z \le 10$	$\psi(x, z, 0) = -90$; $\psi(x, z, 0) = -20$	equations (11) and (12): $S_{wr} = 1/3$, $\phi = 0.45$, $S_s = 0$, $\alpha = -0.01$, $\psi_a = 0$, $\beta = 1; 3$, $\gamma = -1; -3$, $n = 1; 4$	$K_s = 1$ m/d
3S	$\psi = 60 - z$ at $x = 0$, $0 \le y \le 400$, $0 \le z \le 60$; $\psi = 60 - z$ at $x = 1000$, $0 \le y \le 400$, $0 \le z \le 60$; $\psi = 30 - z$ at $x = 540$, $y = 0$; 400, $0 \le z \le 30$; seepage face at $x = 540$, $y = 0$; 400, $30 < z \le 72$	$\psi(x, y, z) = 60 - z$	equation (12): $\alpha = 0.5$, $\psi_a = 0$, $\beta = 2$, $\gamma = 1$, $n = 2$	$K_{sx} = 5$ m/d, $K_{sy} = 2$ m/d, $K_{sz} = 0.5$ m/d
3Ta	$\psi = 60 - z$ at $x = 0$, $0 \le y \le 400$, $0 \le z \le 60$; $\psi = 60 - z$ at $x = 1000$, $0 \le y \le 400$, $0 \le z \le 60$; $\psi = 30 - z$ at $x = 540$, $y = 400$, $0 \le z \le 30$; seepage face at $x = 540$, $y = 400$, $30 < z \le 72$	$\psi(x, y, z, 0) = 60 - z$	equations (11) and (12): $S_{wr} = 0.05$, $\phi = 0.5$, $S_s = 0.01$, $\alpha = 0.5$, $\psi_a = 0$, $\beta = 2$, $\gamma = 1$, $n = 2$	$K_{sx} = 5$ m/d, $K_{sy} = 2$ m/d, $K_{sz} = 0.5$ m/d
3Tb	$K(\psi)((\partial\psi/\partial z) + 1) = -0.00001\ t$ at $z = L$, $0 \le t \le 24$; $K(\psi)((\partial\psi/\partial z) + 1) = -0.00024$ at $z = L$, $24 < t \le t_{min}$; $\psi = \psi_{min}$ at $z = L$, $t_{min} < t \le T_{max}$	$\psi(x, y, z, 0) = L - z$	equations (10) and (8): $\theta_r = 0.04$, $\theta_s = 0.471$, $S_s = 0.001$, $\psi_0 =$ $-0.2806e{-}11$,* $n = 1.176$, $\psi_s = -0.741$	$K_s(z) = K_{s0} \exp(-f(L - z))$, $K_{s0} = K_s(L) = 0.0218$ m/h, $f = 3.526$ m^{-1}, $\psi_{min} = -15$ m
1Tb	$K(\psi)((\partial\psi/\partial z) + 1) = -0.00001\ t$ at $z = L_z$, $0 \le t \le 24$; $K(\psi)((\partial\psi/\partial z) + 1) = -0.00024$ at $z = L_z$, $24 < t \le t_{min}$; $\psi = \psi_{min}$ at $z = L_z$, $t_{min} < t \le T_{max}$	$\psi(z, 0) = L_z - z$; $\psi(z, 0) = -z$	equations (7) and (8): $\theta_r = 0.04$, $\theta_s = 0.471$, $S_s = 0$, $n = 1.176$, $\psi_s = -0.741$	$K_s(z) = K_{s0} \exp(-f(L_z - z))$, $K_{s0} = K_s(L_z) = 0.0218$ m/h, $f = 3.526$ m^{-1}, $\psi_{min} = -15$ m

For test cases 3Tb and 1Tb: L, surface elevation; t_{min}, time at which ψ reaches ψ_{min}.
*Read $-0.2806e{-}11$ as -0.2806×10^{-11}.

The characteristic equations introduced by *van Genuchten and Nielsen* [1985] are commonly used. These can be written as

$$\theta(\psi) = \theta_r + (\theta_s - \theta_r)[1 + \beta]^{-m} \qquad \psi < 0$$
$$\theta(\psi) = \theta_s \qquad \psi \geq 0 \tag{7}$$

$$K_r(\psi) = (1 + \beta)^{-5m/2}[(1 + \beta)^m - \beta^m]^2 \qquad \psi < 0$$
$$K_r(\psi) = 1 \qquad \psi \geq 0 \tag{8}$$

where θ is the volumetric moisture content, θ_r is the residual moisture content, θ_s is the saturated moisture content, $\beta \equiv (\psi/\psi_s)^n$, ψ_s is the capillary or air entry pressure head value, n is a constant, and $m = 1 - 1/n$ for n approximately in the range $1.25 < n < 6$. The corresponding general storage term is

$$\eta = S_w S_s + \phi \frac{dS_w}{d\psi} \tag{9}$$

where $S_w \equiv \theta/\phi$ is the water saturation, ϕ $(= \theta_s)$ is the porosity, and S_s is the specific storage.

A modified version of the *van Genuchten and Nielsen* [1985] $\theta(\psi)$ relationship was introduced by *Paniconi et al.* [1991], who write

$$\theta(\psi) = \theta_r + (\theta_s - \theta_r)[1 + \beta]^{-m}$$
$$\theta(\psi) = \theta_r + (\theta_s - \theta_r)[1 + \beta_0]^{-m} + S_s(\psi - \psi_0)$$
$$\psi < \psi_0$$
$$\psi \geq \psi_0 \tag{10}$$

where ψ_0 is a continuity parameter and $\beta_0 \equiv \beta(\psi_0) = (\psi_0/\psi_s)^n$. The general storage term corresponding to (10) is $\eta = d\theta/d\psi$.

The characteristic equations used by *Huyakorn et al.* [1984] express the water saturation S_w in terms of effective saturation S_e, in the form $S_w(\psi) = (1 - S_{wr})S_e(\psi) + S_{wr}$, where S_{wr} $(= \theta_r/\phi)$ is the residual water saturation. The characteristic relations are then written as

$$S_e(\psi) = [1 + \alpha^\beta(\psi_a - \psi)^\beta]^{-\gamma} \qquad \psi < \psi_a$$
$$S_e(\psi) = 1 \qquad \psi \geq \psi_a \tag{11}$$

$$K_r(\psi) = K_r(S_e(\psi)) = S_e^n \tag{12}$$

where ψ_a is the air entry pressure and α, β, γ, and n are constants. The general storage term is given by (9).

The characteristic equations given above were used in our test simulations. In Table 2 the particular curves used for each test case are indicated, along with the corresponding parameter values.

The method used to evaluate the derivative term in η, and the derivatives of K_r and η needed in the Newton scheme Jacobian, may affect the convergence behavior of the iterative schemes, due to possible discontinuities, steep gradients, and points of inflection in these curves and their derivatives. Numerical differentiation is often used to prevent floating point overflow near singularities or to avoid oscillations around points of inflection. Analytical and various numerical techniques for differentiation of the characteristic equations were investigated in the test simulations. Four different numerical "chord slope" methods were implemented. Method 1 uses the tangent approximation suggested by *Huyakorn et al.* [1984], wherein derivatives are approximated using pressure heads at the current and previous nonlinear iterations. This approximation is used at every iteration and at all nodes, except at nodes where the absolute pressure head difference between iterations is smaller than a specified tolerance, in which case analytical differentiation is used. Chord slope method 2 is the same as method 1, except that when the pressure difference is smaller than the tolerance a centered difference approximation is used. In method 3 the chord slope approximation of method 1 is applied only "locally," at those nodes whose pressure head falls within a specified range. The idea behind this localization approach is that the user, with prior knowledge of the characteristic equations, will know where the troublesome regions of discontinuity, inflection, or sharp gradients are, that is, those regions where it may be most advantageous to use numerical differentiation. Outside these regions analytical differentiation is used. Method 4 follows the same localization idea as method 3, except that rather than use a chord slope formula to differentiate the characteristic equations, a proper tangent slope formula is used, wherein derivatives are approximated using pressure heads at the endpoints of the specified range.

3. Numerical Tests

The physical characteristics and parameter values, with units, for the eight test cases are given in Tables 1 and 2. Table 3 provides a checklist for the various factors and strategies affecting Picard and Newton performance that are examined in the eight test cases. All numerical simulations were run on either an IBM RISC System/6000 model 560 workstation or a Cray Y-MP/864. Where CPU times are reported, they are for the IBM 560.

3.1. Test Case 1S

3.1.1. Description. In test case 1S the effect of an increasing gravity drainage component on Picard and Newton convergence is examined. The gravity drainage zone is defined as the region in a soil column which has zero

Table 3. Factors Affecting Picard and Newton Performance That Are Examined in the Test Cases

Factor/Strategy	1S	1Ta	2S	2T	3S	3Ta	3Tb	1Tb
Problem size			×					
Grid discretization	×		×	×				×
Time discretization; dynamic time stepping		×		×		×	×	×
Boundary conditions; source/sink terms		×		×	×	×		×
Initial conditions; initial solution estimates	×			×				×
Characteristic equations			×	×		×	×	×
Chord slope approximations			×	×		×		
Extent of saturated zones			×				×	×
Convergence tolerance (tol)	×						×	
Convergence error norm			×					
Seepage face convergence criteria						×		
Linear solver				×		×		
Nonlinear relaxation	×		×	×				×
Time weighting				×		×	×	×
Mass lumping				×		×	×	×
Mixed Picard-Newton			×					

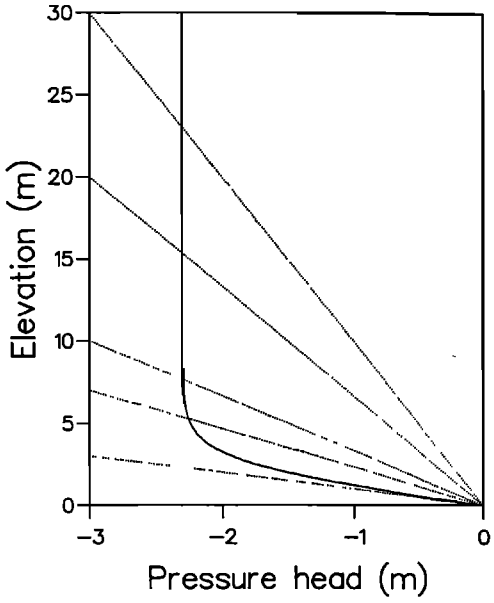

Figure 1. Steady state solution for test case 1S. Dotted lines are the initial solution estimates for the L_z = 3, 7, 10, 20, and 30 m runs. Solid curve to elevation 3 m is the solution for the L_z = 3 run, to 7 m for the L_z = 7 run, and so on.

pressure head gradient (and thus moisture flow is purely gravitational). As the length L_z of the soil column is progressively increased from 3 to 30 m, the extent of the gravity drainage component in the steady state infiltration solution also increases, as is seen in Figure 1.

3.1.2. Results. As can be seen in Figure 2, the Newton scheme converged rapidly, in six or seven iterations, for all five L_z values. Picard convergence, on the other hand, slows as L_z is increased, and the scheme failed to converge for L_z = 30. For the L_z = 20 run, the Picard scheme converged only to a higher tol value of 10^{-9}, rather than to the value 10^{-12} used for all other runs. When applying relaxation (with Ω = 0.2) to the Picard scheme for L_z = 30, convergence was obtained in 127 iterations. Relaxation did not improve, and in some cases worsened, Picard convergence for the other L_z runs. For L_z = 3 the Newton scheme (convergence in seven iterations) required 2.5 CPU s and the Picard scheme (16 iterations) 3.6 s. For L_z = 30, Newton (again seven iterations) required 24.6 s and relaxed Picard (127 iterations) 214.6 s. Mass lumping, a grid discretization of Δz = 0.001 m, and an initial solution estimate of $\psi(z) = -3z/L_z$ were used for all the runs reported in Figure 2. Coarsening the grid to Δz = 0.01 had a negligible effect except for L_z = 30, where unrelaxed Picard converged in 279 iterations, but to a tol value of 10^{-5} only. Changing the initial solution estimate to $\psi(z) = -z$ for $z \leq 3$, $\psi(z) = -3$ for $z > 3$ also made very little difference. The Newton scheme converged in seven iterations for all five L_z values, whereas the Picard scheme converged in 16, 30, and 50 iterations for L_z = 3, 7, and 10, respectively, in 219 iterations (to tol = 10^{-9}) for L_z = 20, and failed for L_z = 30.

3.1.3. Discussion. The gravity drainage zone has a clear impact on the performance of the Picard scheme. A heuristic analysis presented by *Paniconi* [1991] suggests that the derivative of the gravitational gradient component of Richards' equation ($\partial b/\partial\psi$ in (4)), a nonlinear term which is included in the Newton Jacobian but neglected in the Picard scheme, becomes dominant as the extent of the gravity drainage zone increases.

3.2. Test Case 1Ta

3.2.1. Description. The computational efficiency of competing numerical schemes is best evaluated on the basis

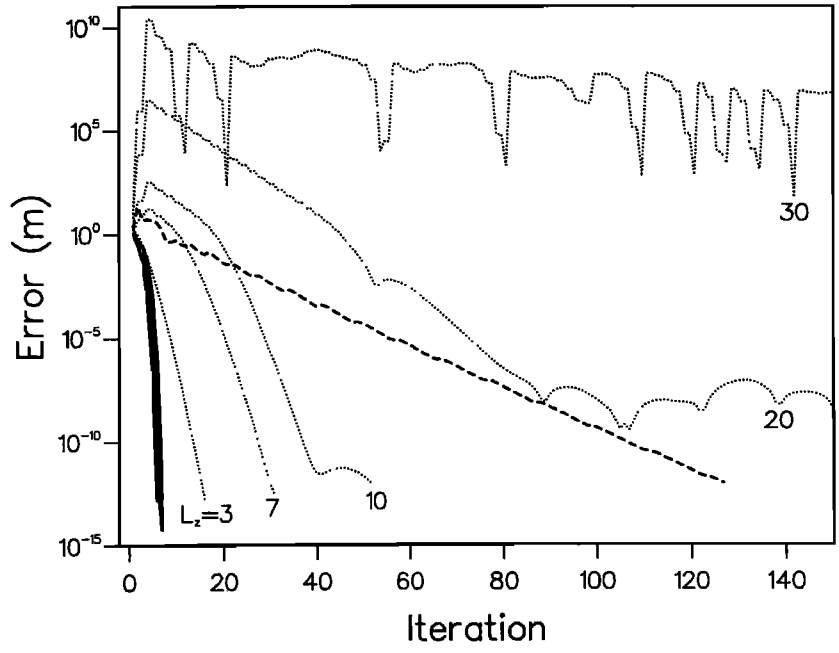

Figure 2. Convergence profiles for test case 1S. Solid curves are the Newton results for the L_z = 3, 7, 10, 20, and 30 m runs, dotted curves are the Picard results for the five runs, and dashed curve is the relaxed Picard result for the L_z = 30 run, with relaxation parameter Ω = 0.2.

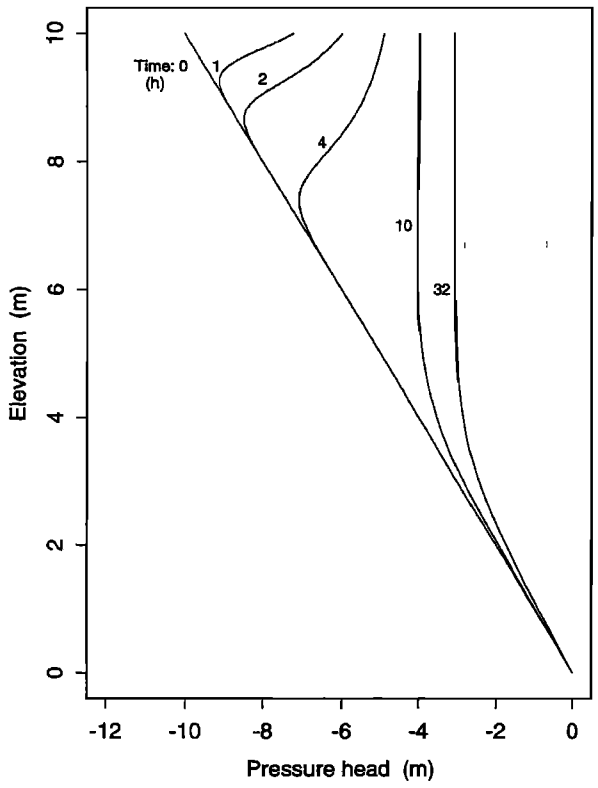

Figure 3. Solution for test case 1Ta at various times.

of CPU time expended to achieve a given level of solution accuracy. Since closed form analytical solutions are nonexistent except for simplified forms of Richards' equation, a numerical solution obtained using a very fine grid and time discretization can be used as a surrogate "exact" solution with respect to which accuracy can be measured. This procedure was used by *Paniconi et al.* [1991] in two test problems to evaluate six linearization methods for the one-dimensional transient Richards equation. The Picard and Newton results from one of these test problems are summarized here. The problem is one of infiltration into a soil column initially at hydrostatic equilibrium, with the infiltration flux increasing linearly with time. A distributed mass matrix and $\lambda = 0.5$ were used. The pressure head profiles at various times are shown in Figure 3.

3.2.2. Results. The Picard and Newton schemes were run repeatedly, each run using a different, constant time step size ranging from 0.005 to 1.0 hour. It was necessary to keep Δt fixed in order to obtain a measure of the accuracy level for each run. The solution accuracy, or numerical error, is given by the difference between the numerical solution and the surrogate exact solution. Plotting the CPU times for each run as a function of these errors (normalized with respect to the exact solution) yields the efficiency plot shown in Figure 4. The superior performance of the Newton scheme for this test case is likely due to the continuous forcing provided by the time-varying boundary condition, which results in sustained slow convergence for the Picard scheme. If the boundary condition were constant (and in the absence of other complicating factors), the Picard scheme would probably converge slowly only during the first few time steps, and more rapidly at later time steps where the solution changes more smoothly between steps. Note in Figure 3 that at later times the solution develops a gravity drainage zone. This may be another factor contributing to the relatively poor performance of the Picard scheme for this test case.

3.2.3. Discussion. The cost of obtaining a fine discretization surrogate exact solution is prohibitive for two- and three-dimensional problems, so the efficiency analysis described above, although straightforward, has not been performed for any of the other test cases. Some of the results from the one-dimensional analysis can be generalized, however, especially considering that the per-iteration CPU cost ratio between the Newton and Picard methods remains approximately constant for one-, two-, and three-dimensional problems. In test case 1Ta, for instance, the Picard scheme required 2–3 times more iterations overall than Newton, and this is roughly the threshold at which the Newton method becomes more efficient than Picard, regardless of the dimensionality of the problem. Another generalization from the procedure described above is that for a given time step value, two schemes with truncation error of the same order do not generally achieve the same accuracy level (related in this case to the asymptotic constant of convergence), and thus an objective measure of computational efficiency is of some importance [*Paniconi et al.*, 1991].

3.3. Test Case 2S

3.3.1. Description. Test case 2S is taken from *Cooley* [1983] and involves steady state flow through a square embankment. *Cooley* [1983] used two grid discretizations and observed slower convergence for the finer grid. This behavior is elaborated here, and the effects of soil characteristics are also examined. A representative solution using

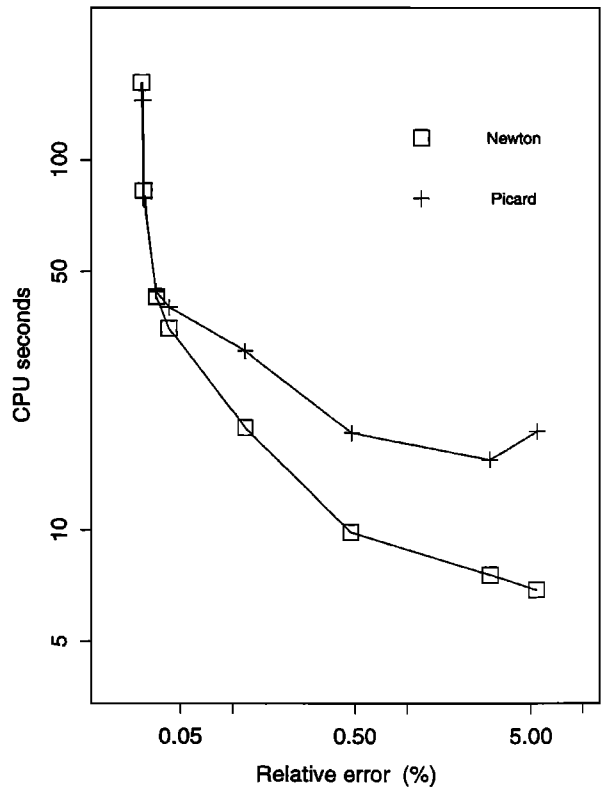

Figure 4. Computational efficiency of the Picard and Newton schemes for test case 1Ta.

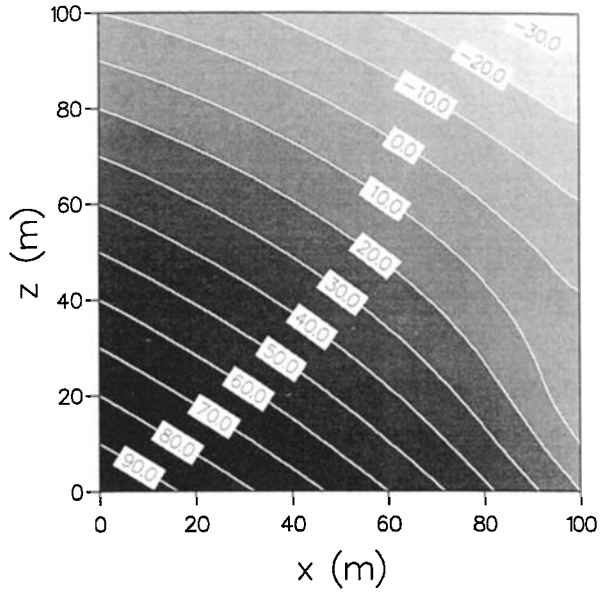

Figure 5. Steady state pressure head contours for test case 2S with grid discretization $\Delta x = \Delta z = 2$ m and equation (12) parameters $\beta = 4$ and $n = 4$.

one of the grid and soil parameter combinations is shown in Figure 5. Attempts were made to enhance the convergence properties of the iterative schemes with relaxation, chord slope approximations, and the mixed Picard-Newton approach. In all simulations, $sf_1 = 0$, $sf_{cvg} = 1$, and a distributed mass matrix were used.

3.3.2. Results. Tables 4 and 5 summarize the convergence results obtained using two $K_r(\psi)$ relationships, with several parameter combinations, and two grid discretizations. The performance of the Picard and Newton schemes deteriorated appreciably for the finer grid in almost all runs, in some cases passing from rapid convergence with the 10-m grid to nonconvergence with the 2-m grid. The mixed Picard-Newton scheme was very effective in overcoming convergence problems at both grid discretizations, in some cases providing rapid convergence where the Picard and/or Newton schemes failed to converge.

The conductivity curves for the range of parameter values

Table 4. Summary of Results for Test Case 2S With $K_r(\psi)$ Relationship (12)

Equation (12) Parameters		Grid Discretization		Number of Nonlinear Iterations			
β	n	Δx	Δz	Picard	Newton	Mixed Picard-Newton	Relaxed Picard
4	4	10	10	21	failed	10+ 15*	35
4	4	2	2	1138	failed	52+ 64	53
2	2	10	10	34	44	14+ 19	
2	2	2	2	78	failed	10+ 27	
1	2	10	10	89	35	10+ 28	
1	2	2	2	87	34	6+ 25	
1	4	10	10	failed	58	9+ 31	44
1	4	2	2	failed	failed	7+ 30	87

*Picard iterations + Newton iterations.

Table 5. Summary of Results for Test Case 2S With $K_r(\psi)$ Relationship (8)

Equation (8) Parameters		Grid Discretization		Number of Nonlinear Iterations		
n	ψ_s	Δx	Δz	Picard	Newton	Mixed Picard-Newton
5	−20	10	10	16	24	6+ 14*
5	−20	2	2	20	29	5+ 19
5	−3	10	10	17	176	8+ 15
5	−3	2	2	74	failed	10+ 33
3	−3	10	10	24	50	8+ 21
3	−3	2	2	74	failed	8+ 30
1.5	−3	10	10	failed	44	9+ 29
1.5	−3	2	2	failed	failed	6+ 29

*Picard iterations + Newton iterations.

used in the two $K_r(\psi)$ relationships are shown in Figure 6. Referring again to the results in Tables 4 and 5, it can be seen that the curves that are most strongly nonlinear (those spanning many orders of magnitude in K_r or having very steep or near-discontinuous gradients around $\psi = 0$) caused the greatest convergence difficulties for the Picard and Newton schemes. As before, the mixed Picard-Newton scheme was very effective in improving convergence behavior.

Nonlinear relaxation and chord slope approximations were tried on the four most difficult cases represented in Table 4: the coarse and fine grid runs for $\beta = 4$, $n = 4$ and $\beta = 1$, $n = 4$. The relaxed Picard results reported in the table are for constant relaxation parameter $\Omega = 0.5$. $\Omega = 1.2$, 0.8, and 0.2, and relaxation with iteration-dependent Ω, all gave worse results than $\Omega = 0.5$. Both fixed and variable Ω relaxation were unsuccessful for the Newton scheme. The convergence profiles for some of the $\beta = 4$, $n = 4$ and $\beta = 1$, $n = 4$ runs are plotted in Figures 7 and 8, showing the dramatic effect that grid discretization, relaxation, and the mixed Picard-Newton scheme can have on the performance of the Picard and Newton methods. Note in Figure 8 the characteristic manner in which the two methods fail: The Picard scheme oscillates within a narrow error band whereas the Newton scheme rapidly diverges.

For steady state simulations, chord slope approximations will only affect the Newton scheme. All four chord slope methods were tried, using a variety of tolerance settings and localization ranges. For the coarse grid $\beta = 1$, $n = 4$ case, for which the Newton scheme converged in 58 iterations, chord slope methods 1 and 2 failed to converge, and methods 3 and 4 gave results similar or much worse than regular Newton, depending on the tolerance value and localization range. In the other three cases the Newton scheme failed to converge, and the chord slope methods also failed, except in two instances for the coarse grid $\beta = 4$, $n = 4$ case, where method 3 converged in 168 iterations and method 4 in 409 iterations.

In Figures 9 and 10 a comparison is shown of the behavior of convergence and residual errors using the l_2 and l_∞ norms. The results are broadly representative in that for most simulations very little difference was observed between

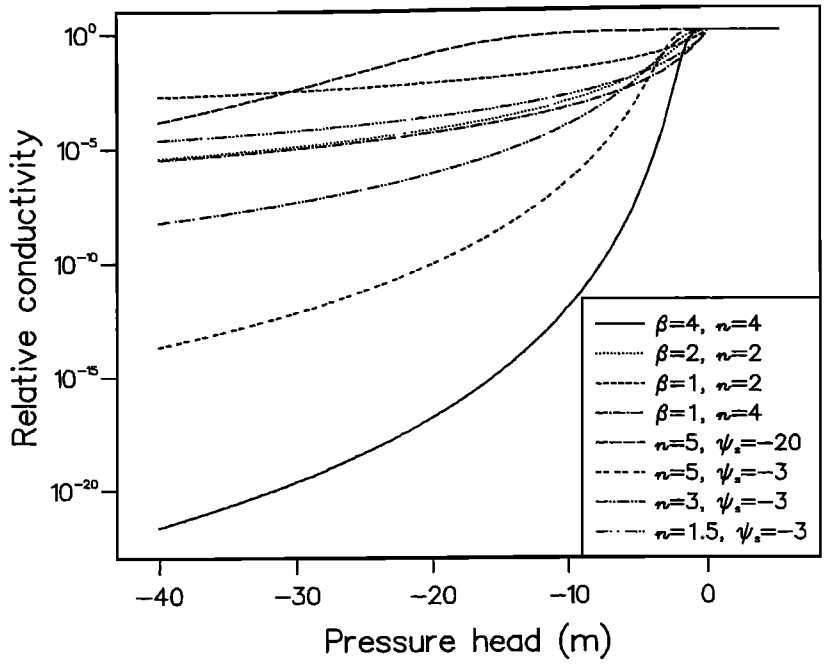

Figure 6. Relative hydraulic conductivity profiles for test case 2S with (12) (parameters β and n) and (8) (parameters n and ψ_s).

the l_2 and l_∞ norms. Moreover, the convergence and residual errors usually followed parallel paths, although exceptions did occur, as seen in Figure 10, and thus it is important to keep track of both errors when checking the convergence of an iterative procedure [*Matthies and Strang*, 1979].

3.3.3. Discussion. Deterioration in Picard and Newton performance when a grid is refined or when the size of a problem is otherwise increased (by an increase in dimensionality, for instance) has been observed for several of the test cases. Although it is not clear what the causes of this behavior are, more often than not they appear to act only during the initial stage of convergence. Typically, this initial stage is characterized by a flat convergence profile, as opposed to the final stage where linear or quadratic convergence can be verified. The initial convergence behavior of both the Picard and Newton schemes is unpredictable and should be studied in greater detail. The difficulties caused by the strong nonlinearities in some of the $K_r(\psi)$ curves were compounded for this test case by the presence of a water table and an extended saturated zone. In particular, the steep and near-discontinuous gradients around $\psi = 0$ result in sharp changes in $K_r(\psi)$ and its derivative across the saturated/unsaturated interface. The chord slope approximations were unable to handle these strong nonlinearities, with only methods 3 and 4 marginally successful. On the other hand, good performance was achieved with nonlinear relaxation for the Picard scheme and with the mixed Picard-Newton approach. A constant value of 0.5 for parameter Ω

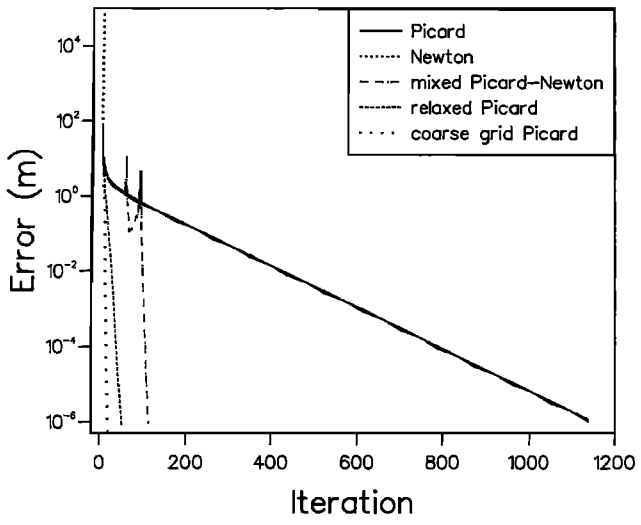

Figure 7. Convergence profiles for test case 2S with equation (12) parameters $\beta = 4$ and $n = 4$.

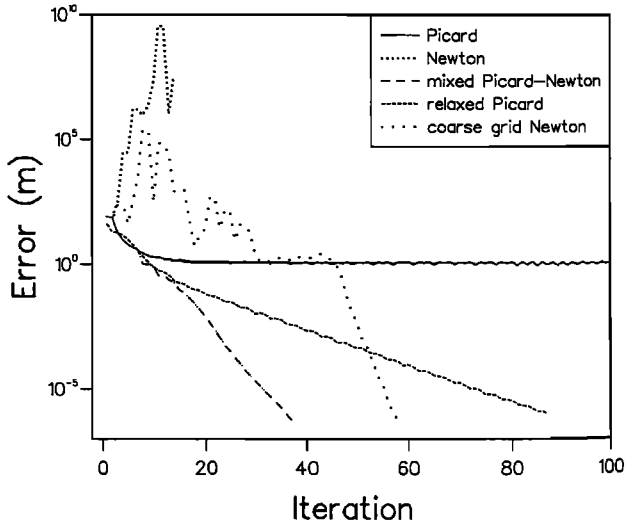

Figure 8. Convergence profiles for test case 2S with equation (12) parameters $\beta = 1$ and $n = 4$.

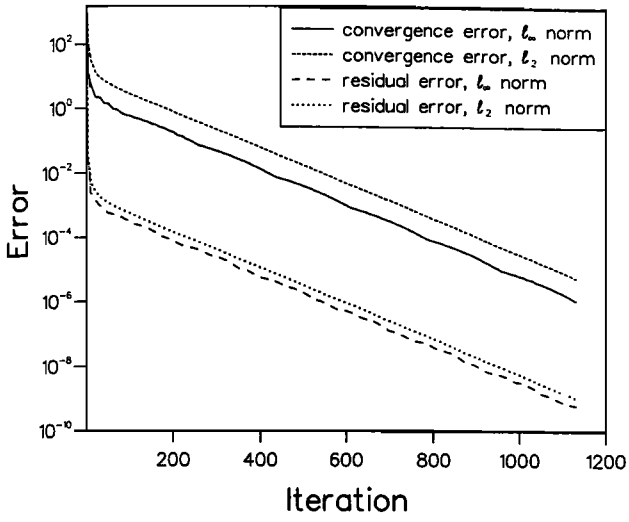

Figure 9. Convergence error (meters) and residual error (square meters per hour) for the Picard simulation of test case 2S with grid discretization $\Delta x = \Delta z = 2$ m and equation (12) parameters $\beta = 4$ and $n = 4$.

worked best for nonlinear relaxation, whereas for the mixed approach the switching from Picard to Newton iteration was done after the convergence error was reduced by 1 order of magnitude, measured relative to the second Picard iteration.

3.4. Test Case 2T

3.4.1. Description. This test case involves two-dimensional transient flow in an unsaturated soil slab. The geometry and configuration for this test case are adapted from *Huyakorn et al.* [1985], where the solution of an associated transport problem is described. The characteristic feature of this test case is the occurrence of convergence difficulties several time steps into the simulation, in response to the buildup of a sharp moisture front near the inflow

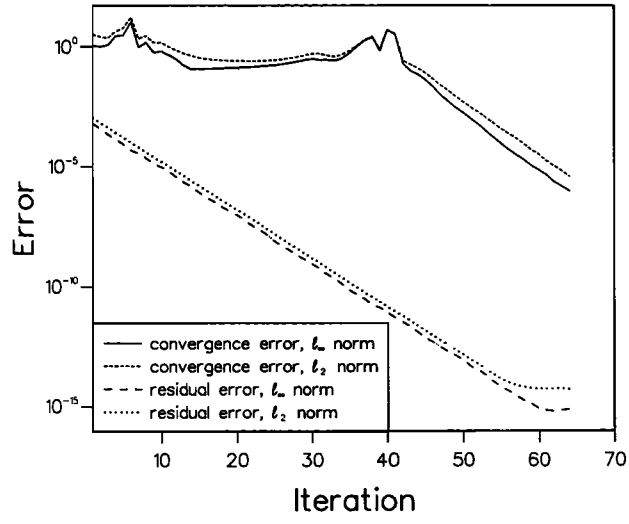

Figure 10. Convergence error (meters) and residual error (square meters per hour) for the Newton iterations in the mixed Picard-Newton simulation of test case 2S with grid discretization $\Delta x = \Delta z = 2$ m and equation (12) parameters $\beta = 4$ and $n = 4$.

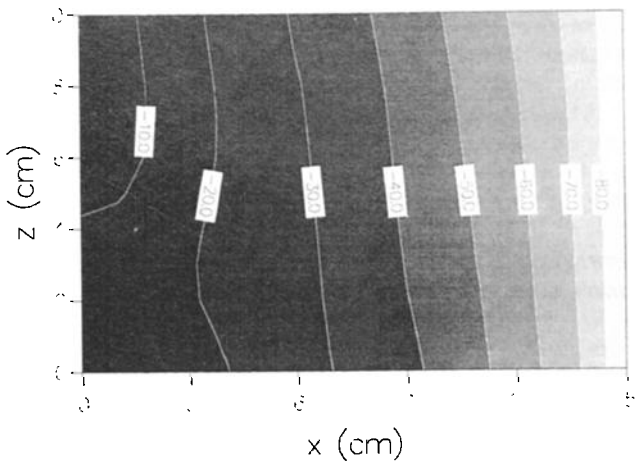

Figure 11. Pressure head contours at time 5 days for test case 2T with grid discretization $\Delta x = \Delta z = 1$ cm and equation (11) and (12) parameters $\beta = 1$, $\gamma = -1$, and $n = 1$.

boundary at $x = 0$, $6 \le z \le 10$. Representative solutions using two soil parameter combinations are shown in Figures 11 and 12. At 5 days the solutions have essentially reached steady state.

3.4.2. Results. The results of 10 Picard and Newton simulations of test case 2T are summarized in Table 6. The parameter values used for the base run are $\lambda = 0.5$, $\Omega = 1$ (no relaxation), $\Delta x = 1$, $\Delta z = 1$, $T_{max} = 5$, $\Delta t_0 = 5 \times 10^{-5}$, $\Delta t_{max} = 1.5$, maxit = 500, $\psi(x, z, 0) = -90$, $\beta = 3$, $\gamma = -3$, and $n = 4$. The values for other parameters are as indicated in Tables 1 and 2. The base run used a distributed mass matrix and no chord slope approximations. After about eight time steps the Picard and Newton schemes began to experience convergence difficulties. At the tenth time step (time 1.0348×10^{-3} day) the Picard scheme required 413 iterations to converge. At its worst the Newton scheme converged in 127 iterations, during the thirteenth step (time 8.4912×10^{-4} day), a better result than Picard, although the Newton method also failed to converge several times during the course of the simulation (four back stepping occurrenc-

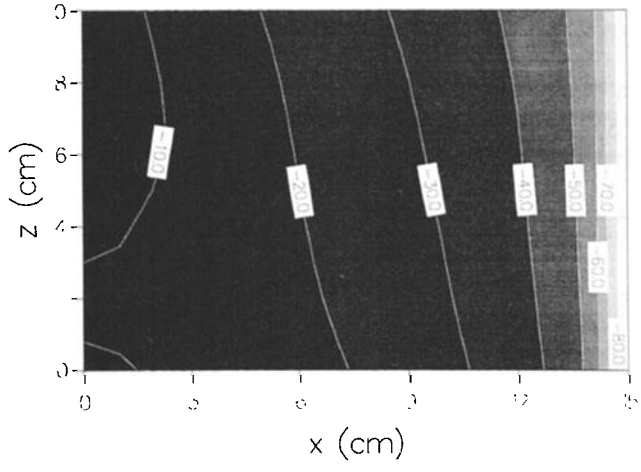

Figure 12. Pressure head contours at time 5 days for test case 2T with grid discretization $\Delta x = \Delta z = 1$ cm and equation (11) and (12) parameters $\beta = 3$, $\gamma = -3$, and $n = 4$.

Table 6. Summary of Results for Test Case 2T

Factor/Strategy	Iteration Scheme	Time Steps	Back Steps	Smallest Δt	Largest Δt	Iterations per Step	Maximum Iterations	CPU Seconds	Comments
Base run	Picard	149	0	5.0e−5*	1.3e−1	12.86	413	55.4	For Picard, 10 iterations per time step toward the end of the simulation. For Newton, three iterations per time step toward the end of the simulation.
	Newton	217	4	1.0e−5	8.0e−1	10.99	127	145.7	
Relaxation with iteration-dependent Ω	Picard	111	0	5.0e−5	6.0e−1	10.04	42	31.4	Relaxation with constant relaxation parameter (Ω = 1.2, 0.8, 0.5, 0.2) performed poorly.
	Newton	230	3	1.9e−5	1.1	10.27	60	97.5	
Backward Euler time differencing (λ = 1.0)	Picard	failed	4						Picard failed to converge during first time step, with back stepping until $\Delta t = \Delta t_{min}$ reached. For Newton, small time step sizes required for most of the simulation, except toward the end.
	Newton	316	0	3.0e−5	1.1	10.32	31	118.1	
Chord slope method 1 with tolerance 1.0e−8	Picard	238	0	5.0e−5	1.3e−1	10.81	25	70.5	Picard showed similar behavior for other chord slope methods. Newton showed similar behavior for chord slope method 2. Methods 3 and 4 performed poorly.
	Newton	256	0	1.0e−5	8.0e−1	12.38	118	109.0	
Mass lumping	Picard	106	2	5.0e−5	3.8e−1	9.36	12	65.8	Back stepping near the end of the Picard simulation, due to time step sizes becoming too large. No trouble with the large time step sizes toward the end of the Newton simulation.
	Newton	165	0	5.0e−5	8.2e−1	9.56	13	59.3	
Initial conditions $\psi(x, z, 0) = -20$	Picard	57	0	5.0e−5	1.1	8.21	12	14.0	Two iterations per time step towards the end of the Picard simulation. Newton had trouble during first time step, then performance very similar to Picard.
	Newton	62	0	3.0e−5	1.2	9.34	73	21.7	
Linear $K_r(\psi)$, $S_e(\psi)$ ($\beta = 1$, $\gamma = -1$, $n = 1$)	Picard	20	0	5.0e−2	5.3e−1	9.85	13	7.0	Picard was insensitive to Δt_0 ($\Delta t_0 = 0.5$ was also successful). Newton was sensitive to Δt_0, but larger time step sizes achieved toward the end of the simulation.
	Newton	50	5	3.9e−3	1.2	9.72	20	81.8	
Variable time step size, $\Delta t_0 = 0.1$	Picard	128	0	2.2e−2	1.0e−1	11.64	42	49.1	Picard solution exhibits oscillations, also when mass lumping is used (see Figure 13). Newton solution is oscillation-free (see Figure 13), but note large number of back steps.
	Newton	161	7	2.8e−3	8.5e−1	10.22	21	61.5	
Fine grid (Δx = 0.25), T_{max} = 0.005	Picard	41	4	6.5e−6	3.9e−4	10.95	29	78.2	Convergence problems occur earlier in the simulation due to finer grid (initial sharp front is at $x = 0.25$ rather than at $x = 1.0$).
	Newton	79	5	1.0e−6	1.5e−4	13.67	111	177.4	
Constant time step size, T_{max} = 0.01	Picard	1000	0	1.0e−5	1.0e−5	3.37	20	84.0	Picard had average of eight linear solver iterations per nonlinear iteration; Newton had average of four linear solver iterations per nonlinear iteration.
	Newton	1000	0	1.0e−5	1.0e−5	3.84	21	121.0	

*Read 5.0e−5 as 5.0×10^{-5}.

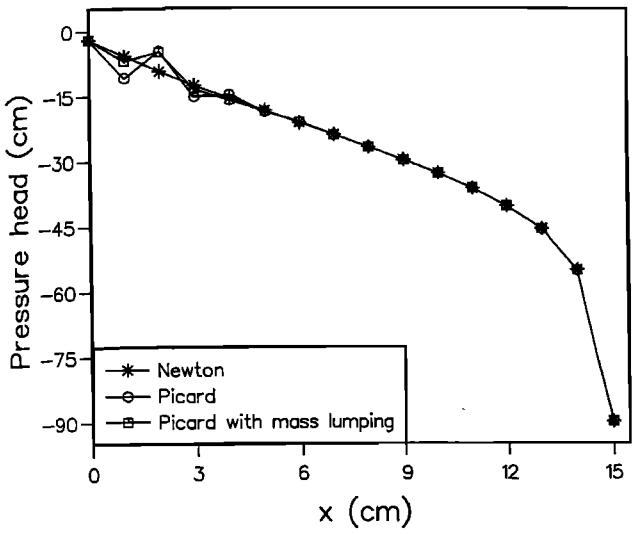

Figure 13. Pressure head profiles at time 5 days, cross section $z = 8$ cm for test case 2T with $\Delta t_0 = 0.1$ days, grid discretization $\Delta x = \Delta z = 1$ cm, and equation (11) and (12) parameters $\beta = 3$, $\gamma = -3$, and $n = 4$.

es). Toward the end of the simulation the Newton method performed better than Picard, requiring fewer iterations per step and achieving higher time step sizes. However, due to Δt reductions during back stepping, the Newton run required significantly more time steps overall than the Picard run. Note that comparing the Picard and Newton CPU times in Table 6 is meaningful only for those runs where neither scheme back stepped, since with back stepping the CPU times include the cost of failed convergence, which is an arbitrary cost dependent on the value of maxit. Also note that the average iterations per time step reported in the table do not include iterations during failed time steps.

The base run conditions were altered in various ways for the other nine Picard and Newton simulations. Unlike test case 2S, relaxation with iteration-dependent Ω performed well here while relaxation with constant Ω did not. The backward Euler scheme ($\lambda = 1.0$) and chord slope approximations did not yield significant improvements over the base run. Mass lumping was able to reduce oscillations at the sharp moisture front, thus resulting in good convergence for both the Picard and Newton schemes. The biggest improvements over the base run came about by reducing the severity of the sharp front, either by making the pressure head drop across the front smaller (changing the initial conditions to $\psi(x, z, 0) = -20$) or by using smoother characteristic equations ($\beta = 1$, $\gamma = -1$, $n = 1$). Both these measures produce smaller jumps in the nonlinear coefficients $K_r(\psi)$ and $S_e(\psi)$ (and their derivatives) across the sharp front, and a $K_r(\psi)$ that is more permeable to water on the dry side of the front. Smoother $S_e(\psi)$ and $K_r(\psi)$ curves were tried for illustrative purposes only, since altering the characteristic equations changes the physical problem that is being solved (compare Figures 11 and 12). The use of a larger initial time step size ($\Delta t_0 = 0.1$) was an attempt to avoid the trouble area encountered in the base run at around time 0.001 day. However, convergence troubles were merely shifted to later times, and the end result was still a large number of time steps overall. Moreover, the Picard method (with and without mass lumping) produced an oscillatory solution, as can be seen in Figure 13, whereas the Newton solution was oscillation-free, owing to back stepping–induced smaller time steps early in the simulation. The fine grid case ($\Delta x = 0.25$, $\Delta z = 1.0$) was only run to $T_{max} = 0.005$. Both Picard and Newton performed poorly for this case, in a manner similar to the behavior seen in other test cases for fine grids. The constant time step run ($\Delta t = 10^{-5}$) to $T_{max} = 0.01$ allowed a step by step comparison of the Picard and Newton schemes. Convergence was slightly better for the Picard scheme, and Picard required 30% less CPU time.

3.4.3. Discussion. The combination of soil parameters and boundary and initial conditions used in the base run produces a sharp moisture front with a large drop in conductivity and saturation across the front. These conditions create convergence difficulties for the Picard and Newton scheme which can be alleviated to some extent by using lumped rather than distributed mass matrices. This test case is a good illustration of both the utility and limitations of dynamic time stepping and back stepping. For instance, in the Newton base run, which required 145 s of CPU, Δt ranged over almost 5 orders of magnitude during the course of the simulation. Running the 5-day simulation at the time step size needed to overcome the early convergence difficulties, $\Delta t = 10^{-5}$, would have required approximately 18 hours of CPU. On the other hand, in the Picard simulation with $\Delta t_0 = 0.1$, the time step control mechanisms were not sufficient to guarantee an accurate (oscillation-free) solution.

3.5. Test Case 3S

3.5.1. Description. This test case is taken from *Huyakorn et al.* [1986] and involves three-dimensional flow in a pumped unconfined aquifer. The grid discretization in the x and z directions is nonuniform, while in the y direction it is uniform with $\Delta y = 50$ m. The grid nodes in the x direction are located at $x = 0$, 70, 120, 160, 200, 275, 350, 400, 450, 500, 540, 570, 600, 650, 700, 750, 800, 850, 900, 950, and 1000 m. In the z direction the nodes are at $z = 0$, 15, 30, 35, 40, 45, 50, 55, 60, 66, and 72 m. The pumping well is simulated via three Dirichlet nodes, at $z = 0$, 15, and 30 m, with a seepage face above these nodes ($30 < z \leq 72$). The flow problem is solved under both steady state (this test case) and transient (test case 3Ta) conditions. In the steady state case a curious effect of well positioning is illustrated. Two runs are performed, run 1 with the pumping well at $x = 540$ m, $y = 400$ m and run 2 with the well at $x = 540$ m, $y = 0$ m. The solution contours at cross section $y = 400$ m for the first run are shown in Figure 14. For both runs, $sf_1 = 0$, $sf_{cvg} = 1$, and a distributed mass matrix were used.

3.5.2. Results. The solutions for runs 1 and 2 are exact mirror images of each other since the grid discretization in the y direction is uniform and since, apart from the well position, the boundary conditions at $y = 400$ and $y = 0$ are identical. However, as shown in Figure 15, the Newton scheme took nearly twice as many iterations to converge for run 1 as for run 2. The same node numbering sequence was used for both runs, and thus different node numbers got assigned to the pumping well for the two runs. This produced a slight structural difference in the coefficient matrices of the discretized system, which apparently affected the initial convergence behavior of the Newton scheme. During the final stage of convergence, the two Newton runs, and also

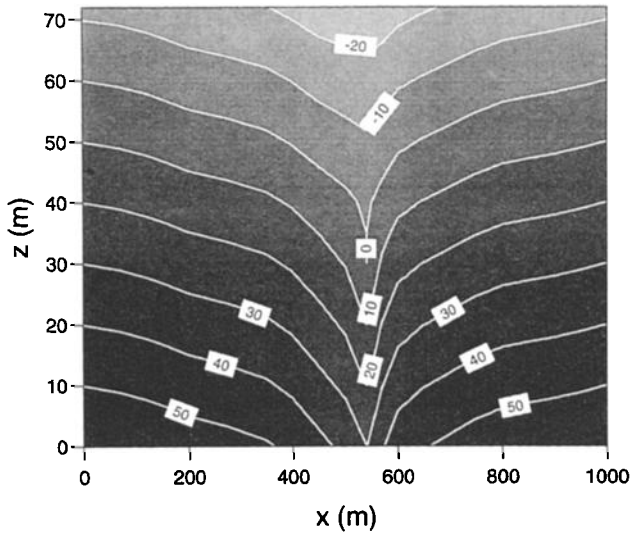

Figure 14. Steady state pressure head contours at cross section $y = 400$ m for test case 3S with the pumping well at $x = 540$ m, $y = 400$ m.

the Picard runs, displayed very similar behavior, converging in 9–13 iterations (Figure 15).

3.5.3. An aside. *Huyakorn et al.* [1986] reported that 177 min of CPU were needed for six Picard iterations in single precision on a VAX model 11/750 minicomputer. On the IBM 560 RISC workstation, 15 Picard iterations in double precision required 9 s of CPU, which is more than 3000 times faster than the simulations run a mere 8 years ago.

3.6. Test Case 3Ta

3.6.1. Description. The flow problem described in test case 3S is solved here under transient conditions. The simulations were run to $T_{max} = 5000$ days using the time discretization parameters given in Table 1. Very small time step sizes were needed initially ($\Delta t_0 = 2 \times 10^{-5}$ day), but as the solution approached steady state (after approximately 3000 days), the time step sizes increased to $\Delta t_{max} = 100$ days. Oscillations along the rapidly changing saturated/unsaturated interface near the seepage face caused convergence problems early in the simulations. Various strategies were tried in attempts to overcome these convergence difficulties.

3.6.2. Results. Only the backward Euler scheme ($\lambda = 1.0$) was effective in overcoming the nonlinear convergence oscillations near the seepage face. With $\lambda = 0.5$ both the Picard and Newton schemes failed to converge, with and without chord slope approximations and with and without mass lumping. The troubles occurred during the first two time steps, and included repeated nonconvergence of the seepage face exit point, regardless of the values of sf_1 and sf_{cvg}. With $\lambda = 1.0$, successful convergence was achieved for both iterative methods, again with no apparent effect of parameters sf_1 and sf_{cvg} (all four combinations of these two parameters were tried). Other strategies also had a minor effect on the performance of the Newton and Picard schemes. Mass lumping was slightly more efficient than the distributed case, and the chord slope approximations gave noticeably worse results than not using these approximations. For the chord slope methods a tolerance setting of 10^{-5} was used, and methods 1 and 2 gave identical results.

The results of several of the runs described above are summarized in Table 7. The BICGSTAB linear solver was used for the Newton runs reported in the table. Other nonsymmetric solvers were also tried (GRAMRB, GCRK, and TFQMR), but none of these was as efficient as BICGSTAB, requiring, in the best case, 50% more iterations and CPU time.

Overall, the Picard scheme converged faster and was more efficient than the Newton scheme. For this test case the CPU time per nonlinear iteration required for the Picard scheme was approximately 0.32 s, and for the Newton scheme approximately 0.60 s. The breakdown of the total CPU cost for one of the Picard and Newton runs for this test case is shown in Figure 16. This cost distribution, which is typical for the multidimensional transient simulations performed in this and other test cases, shows that for both the Picard and Newton schemes, over half the CPU time is used in solving the linearized system of equations. The next most intensive kernel, requiring about one quarter of the total CPU time, is the calculation and assembly of the finite element system matrices, including the Jacobian matrix for the Newton scheme. All the other tasks combined use up only 15–20% of the total CPU time.

3.6.3. Related results. *Putti and Paniconi* [1992] considered a variant of test case 3Ta. The test problem was modified to include prevailing flow along the x direction. Variable and fixed time step size simulations were run, and characteristic equations (7) and (8) were used in addition to (11) and (12). For some of the time steps in these tests the Picard scheme had trouble converging while the Newton method converged rapidly. Chord slope approximations applied to the Picard scheme increased its rate of convergence, although yielding very irregular or oscillatory convergence profiles.

3.7. Test Case 3Tb

3.7.1. Description. This test case involves the simulation of an evaporation event on a subcatchment of the Konza

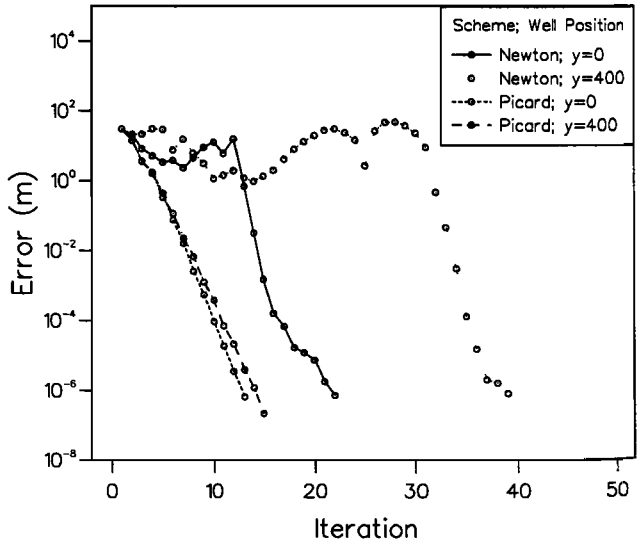

Figure 15. Convergence profiles for test case 3S showing the effect of pumping well position.

Table 7. Summary of Results for Test Case 3Ta

Iteration Scheme	λ	Mass Lumping	Chord Slope Approximation	Time Steps	Back Steps	Nonlinear Iterations per Time Step	Linear Iterations per Nonlinear Iteration	CPU Seconds
Picard	0.5	yes	no	failed				
Newton	0.5	yes	no	failed				
Picard	0.5	no	no	failed				
Newton	0.5	no	no	failed				
Picard	0.5	yes	yes	failed				
Newton	0.5	yes	yes	failed				
Picard	1	yes	no	178	0	5.31	9.08	304
Newton	1	yes	no	178	0	7.92	5.00	849
Picard	1	no	no	178	0	5.80	10.66	362
Newton	1	no	no	184	0	9.35	5.04	1065
Picard	1	no	yes	178	0	7.19	10.01	435
Newton	1	no	yes	186	1	10.83	4.78	1222

Prairie reserve in northeastern Kansas. The catchment, the numerical model, and the observation data used to parameterize the model are described by *Paniconi and Wood* [1993]. The model differs from the one used for test cases 3S and 3Ta in that hexahedral elements are used and the nonlinear system integrals are evaluated by Gaussian quadrature. The grid discretization in the x and y directions is uniform with $\Delta x = \Delta y = 30$ m. Vertically, the catchment is discretized into 25 layers of increasing thickness from the surface to the base, with $\Delta z = 0.002$ (surface layer), 0.002, 0.002, 0.004, 0.004, 0.005, 0.005, 0.01, 0.01, 0.01, 0.02, 0.02, 0.02, 0.04, 0.04, 0.046, 0.05, 0.05, 0.06, 0.1, 0.1, 0.1, 0.1, 0.1, and 0.1 m (base layer). The saturated hydraulic conductivity is vertically heterogeneous, with the distribution of values given by the exponential relationship in Table 2. The evaporation flux at the surface of the catchment increases uniformly from 0.0 to -0.00024 m/h for the first 24 hours of simulation, and then remains constant at -0.00024 m/h until the pressure head at a surface node becomes smaller than the air-dry value $\psi_{min} = -15.0$ m, at which point the boundary condition at that node switches from specified flux to constant head. In Figure 17 the vertical solution profiles at a selected point on the catchment are shown at various times. From these profiles it can be seen that the surface becomes air-dry at a time between 200 and 500 hours.

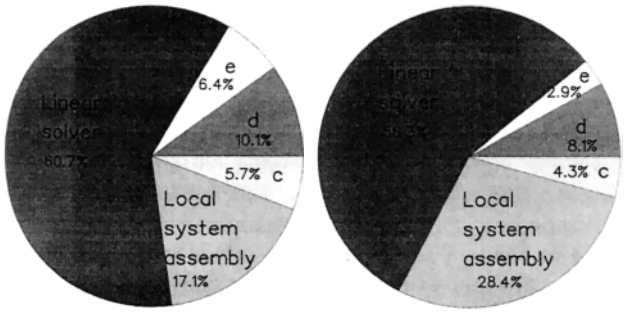

Figure 16. Test case 3Ta CPU distributions for the (left) Picard and (right) Newton schemes. Here c denotes evaluation and differentiation of characteristic equations; d, program overhead (including initialization, setting of boundary conditions, calculation of the right-hand side vector, and convergence checking); and e, calculation of mass balance errors and updating of seepage faces.

3.7.2. Results. Two sets of simulations were run for this test case, one using $T_{max} = 30{,}000$ hours, $\Delta t_0 = 1$ hour, $\Delta t_{max} = 200$ hours, and tol $= 5 \times 10^{-2}$ and the other using $T_{max} = 336$ hours, $\Delta t_0 = 0.1$ hour, $\Delta t_{max} = 12$ hours and tol $= 5 \times 10^{-4}$, with all other parameters as indicated in Tables 1 and 2. Of the two tol values, tol $= 5 \times 10^{-2}$ represents the less stringent accuracy requirement, and for this set of simulations a very large time discretization could be used without incurring convergence difficulties and back stepping costs.

For the tol $= 5 \times 10^{-4}$ simulations, much smaller time step sizes were required, and severe convergence troubles were encountered. The results for this second set of simulations are summarized in Table 8 and show that for many time steps the Picard and Newton schemes failed to converge (the number of back stepping occurrences for each run ranged from 29 to 162). The convergence troubles occurred

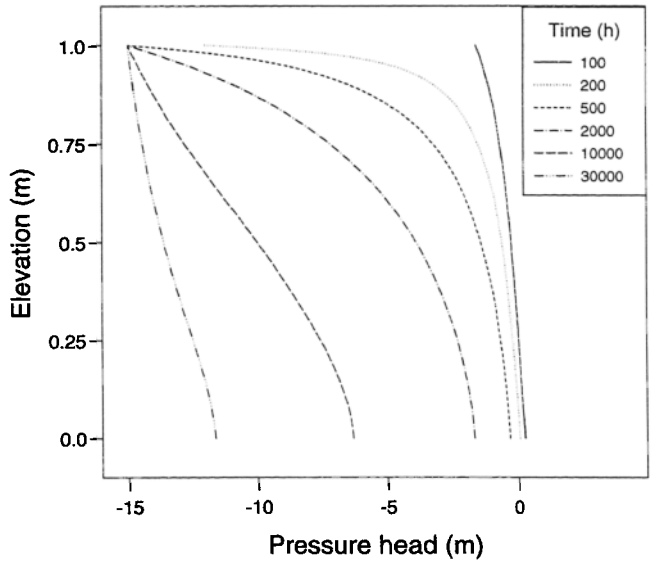

Figure 17. Vertical pressure head profiles at $x = 150$ m, $y = 360$ m for test case 3Tb. Similar profiles were obtained for test case 1Tb.

Table 8. Summary of Results for Test Case 3Tb With T_{max} = 336 Hours, Δt_0 = 0.1 Hour, Δt_{max} = 12 Hours, and tol = 5×10^{-4}

Iteration Scheme	λ	Mass Lumping	Time Steps	Back Steps	Nonlinear Iterations per Time Step
Picard	0.5	yes	198	44	4.05
Newton	0.5	yes	144	29	3.33
Picard	1	yes	246	57	4.21
Newton	1	yes	172	37	3.37
Picard	0.5	no	533	136	3.39
Newton	0.5	no	365	90	2.98
Picard	1	no	628	162	3.47
Newton	1	no	409	102	3.11

in the early stages of simulation and diminished as the soil became drier. In fact, these troubles were directly related to the extent of the saturated zone and were due to pressure head oscillations at nodes along the water table and in the saturated zone. The characteristic equations used for these simulations, in particular the $K_r(\psi)$ curve, are strongly nonlinear with steep gradients around $\psi = 0$. After the water table dropped below the base of the catchment and the soil became entirely unsaturated (around time 250 hours), convergence became much more rapid, and the time step sizes increased steadily to Δt_{max}. As can be seen in Table 8, the Newton scheme had less difficulty converging than Picard for these runs, Crank-Nicolson time weighting ($\lambda = 0.5$) gave somewhat better performance than the backward Euler scheme, and lumped mass matrices gave much better results than distributed mass matrices.

3.7.3. Discussion. As in test case 3Ta these simulations experienced convergence difficulties due to oscillations near the saturated/unsaturated interface. Unlike test case 3Ta, where backward Euler time weighting was necessary to achieve convergence, in this test case the Crank-Nicolson scheme was also successful. In test case 3Ta, convergence failures occurred only during the first two time steps, and the changes in pressure head around the seepage face were probably more sudden (in response to well pumping) than the water table changes in test case 3Tb in response to slowly varying evaporation fluxes.

For simulations that exhibit pressure head oscillations during an iterative procedure, the convergence check can be modified to detect such oscillations, thereby avoiding needlessly iterating maxit times. A trickier aspect of oscillation-related convergence failure is that the dynamic time stepping procedure does not always work in an optimal fashion for such cases. Convergence can be very rapid at one time step and oscillatory the next, so the strategy of gradually increasing the time step size so long as convergence is rapid can result in repeated occurrences of back stepping. This behavior is reflected in Table 8, where many back steps occurred in tandem with a rather small average number of nonlinear iterations per time step.

3.8. Test Case 1Tb

3.8.1. Description. In this test case, one-dimensional simulations are run at a selected point on the catchment of test case 3Tb. For a 30,000-hour simulation the same solution profiles obtained for test case 3Tb apply (see Figure 17), although only 336-hour simulations are reported here. The $K_r(\psi)$ relationship for this test case is the same as the one used for the previous test case, and thus similar convergence problems, owing to the strong nonlinearity of this curve near $\psi = 0$, are to be expected. In reality, however, the convergence difficulties are much greater for this test case, because characteristic equation (7) with $S_s = 0.0$ is used rather than (10) with $S_s = 0.001$. This combination results in a discontinuous $dS_w/d\psi$ curve at $\psi = 0$ and a general storage term η which is zero in the saturated zone. With $\eta = 0$ for $\psi > 0$ the governing equation (1) changes from a parabolic equation to an elliptic one across the saturated/unsaturated interface. Three grid discretizations and two initial conditions were tried in attempts to overcome these convergence difficulties. Two of the grid discretizations were uniform, with Δz = 0.04 m for one set of runs and Δz = 0.002 m for the other. The third discretization is the same nonuniform one used in test case 3Tb. Both initial conditions were hydrostatic, with the first one, $\psi(z, 0) = L_z - z$, resulting in a fully saturated column and the second, $\psi(z, 0) = -z$, being completely unsaturated except for the node at $z = 0$.

3.8.2. Results. The results for this test case are summarized in Table 9. With saturated initial conditions, very poor performance was obtained for both the Picard and Newton schemes for all three grid discretizations. None of the Newton runs converged, and only a few of the Picard runs were successful, although a very small Δt_{min} (10^{-6} hour) was needed and many back steps occurred. Nonlinear relaxation was also tried for these runs, but without success. With unsaturated initial conditions both the Picard and Newton schemes converged easily and without back stepping, with Newton converging a little faster than Picard. Crank-Nicolson time weighting gave slightly better performance than the backward Euler scheme, while lumped and distributed mass matrices gave nearly identical results.

3.8.3. Discussion. With saturated initial conditions the governing equation is completely elliptic during the first iterations of the first time step (it does not remain so for very long due to the evaporation boundary condition which quickly produces unsaturated nodes and hence nonzero storage coefficients). A unique solution is not guaranteed for an elliptic equation with only flux boundary conditions specified. This was likely a factor, in addition to the previously described characteristic equation-related convergence problems, in the very poor performance of the Picard and Newton schemes for the runs with saturated initial conditions.

4. Conclusions

Numerical procedures for solving large-scale nonlinear problems are computationally intensive and require highly efficient and robust algorithms. Efficiency ensures optimal utilization of CPU and storage resources to attain a desired level of solution accuracy, while robustness implies that a given algorithm exhibits acceptable convergence behavior across a wide spectrum of simulation scenarios. The two most commonly used iterative procedures for solving Richards' equation, the Picard and Newton schemes, have been tested in a series of finite element simulations of flow in variably saturated porous media. Steady state and transient simulations in one-, two-, and three-dimensional media were conducted. Various factors affecting the efficiency and robustness of the Picard and Newton methods were investi-

Table 9. Summary of Results for Test Case 1Tb

Initial Conditions	Grid Discretization	Number of Elements	Iteration Scheme	λ	Mass Lumping	Time Steps	Back Steps	Nonlinear Iterations per Time Step	CPU Seconds
$\psi(z, 0) = L_z - z$	uniform, $\Delta z = 0.04$	25	Picard	0.5	yes	128	20	3.44	2.21
$\psi(z, 0) = L_z - z$	uniform, $\Delta z = 0.04$	25	Newton	0.5	yes	failed			
$\psi(z, 0) = L_z - z$	uniform, $\Delta z = 0.04$	25	Picard	1	yes	164	22	6.10	3.27
$\psi(z, 0) = L_z - z$	uniform, $\Delta z = 0.04$	25	Picard	0.5	no	failed			
$\psi(z, 0) = L_z - z$	uniform, $\Delta z = 0.04$	25	Picard	1	no	failed			
$\psi(z, 0) = L_z - z$	uniform, $\Delta z = 0.002$	500	Picard	0.5	yes	64	1	4.88	9.49
$\psi(z, 0) = L_z - z$	uniform, $\Delta z = 0.002$	500	Newton	0.5	yes	failed			
$\psi(z, 0) = L_z - z$	nonuniform, $\Delta z = [0.002, 0.1]$	25	Picard	0.5	yes	64	3	4.28	0.96
$\psi(z, 0) = L_z - z$	nonuniform, $\Delta z = [0.002, 0.1]$	25	Newton	0.5	yes	failed			
$\psi(z, 0) = -z$	nonuniform, $\Delta z = [0.002, 0.1]$	25	Picard	0.5	yes	56	0	4.34	0.72
$\psi(z, 0) = -z$	nonuniform, $\Delta z = [0.002, 0.1]$	25	Newton	0.5	yes	56	0	2.66	0.76
$\psi(z, 0) = -z$	nonuniform, $\Delta z = [0.002, 0.1]$	25	Picard	1	yes	56	0	4.98	0.74
$\psi(z, 0) = -z$	nonuniform, $\Delta z = [0.002, 0.1]$	25	Newton	1	yes	56	0	2.79	0.78
$\psi(z, 0) = -z$	nonuniform, $\Delta z = [0.002, 0.1]$	25	Picard	0.5	no	56	0	4.34	0.68
$\psi(z, 0) = -z$	nonuniform, $\Delta z = [0.002, 0.1]$	25	Newton	0.5	no	56	0	2.66	0.72
$\psi(z, 0) = -z$	nonuniform, $\Delta z = [0.002, 0.1]$	25	Picard	1	no	56	0	4.93	0.76
$\psi(z, 0) = -z$	nonuniform, $\Delta z = [0.002, 0.1]$	25	Newton	1	no	56	0	2.77	0.78

gated. These factors are indicated in Table 3, and their effects illustrated and summarized in the tables and figures for each of the test cases referred to in Table 3. We make a few additonal remarks here.

In many cases the Picard scheme converges well, and in such cases it is clearly the simplest and most efficient method for linearizing Richards' equaton. However, there are cases where the Picard scheme fails to converge or converges very slowly. We note in particular the difficulties encountered with gravity drainage zones, complex time-varying boundary conditions, strongly nonlinear characteristic equations, and saturated/unsaturated interfaces. Relaxation is sometimes successful in overcoming these convergence troubles, with the minor drawback that one has to choose an appropriate value for the relaxation parameter Ω, either empirically after every iteration or as an a priori constant. The various chord slope approximations were not very effective, and, like relaxation, additional parameters need to be specified (tolerance levels, localization regions). The Newton scheme is generally more robust and faster converging than Picard, although it too can fail to converge, in some cases for the same reasons as Picard (strongly nonlinear characteristic equations and saturated/unsaturated interfaces), and in other cases due to poor initial solution estimates. The mixed Picard-Newton approach can effectively overcome the Newton scheme's sensitivity to initial solution estimates, but it has the disadvantage of requiring both symmetric and nonsymmetric storage modes (unless the Picard scheme is stored and solved as a nonsymmetric system). This mixed approach requires further study to establish an optimal criterion for switching from Picard to Newton iteration.

In future work the effects of heterogeneity on convergence behavior, not addressed in this paper, will be investigated. Other approaches to solving nonlinear equations will be implemented, such as modified Newton, quasi-Newton, implicit factored, and explicit multigrid schemes [*Ortega and Rheinboldt*, 1970; *Dennis and Moré*, 1977; *Paniconi et al.*, 1991; *Putti et al.*, 1990]. Three of these methods seek to reduce the costs associated with Newton iteration by selectively updating the Jacobian (modified Newton), approximating the inverse Jacobian (quasi-Newton), or evaluating the full Jacobian but not iterating (implicit factored). The fourth uses an explicit time stepping scheme, along with a multigrid algorithm to alleviate the time step constraint needed to preserve stability.

Acknowledgments. This research has been carried out with the financial support of the Sardinia Regional Authorities, CINECA (contract 92-1-104-1), and the Italian CNR (Gruppo Nazionale per la Difesa dalle Catastrofi Idrogeologiche, linea di Ricerca 4). Test case 1S was conducted in collaboration with Rachid Ababou, with financial support from the Southwest Research Institute, San Antonio, Texas.

References

Ababou, R., L. W. Gelhar, and D. McLaughlin, Three-dimensional flow in random porous media, 2 vol., *Rep. 318*, Ralph M. Parsons Lab., Mass. Inst. of Technol., Cambridge, 1988.

Aldama, A. A., and C. Paniconi, An analysis of the convergence of Picard iterations for implicit approximations of Richards' equation, in *Proceedings of the IX International Conference on Computational Methods in Water Resources*, edited by T. F. Russell, R. E. Ewing, C. A. Brebbia, W. G. Gray, and G. F. Pinder, pp. 521–528, Computational Mechanics Publications, Billerica, Mass., 1992.

Ames, W. F., *Numerical Methods for Partial Differential Equations*, 2nd ed., Academic, San Diego, Calif., 1977.

Axelsson, O., Conjugate gradient type methods for unsymmetric and inconsistent systems of linear equations, *Linear Algebra Appl.*, *29*, 1–16, 1980.

Brutsaert, W., A functional iteration technique for solving the Richards equation applied to two-dimensional infiltration problems, *Water Resour. Res.*, *7*(6), 1583–1596, 1971.

Celia, M. A., E. T. Bouloutas, and R. L. Zarba, A general mass-conservative numerical solution for the unsaturated flow equation, *Water Resour. Res.*, *26*(7), 1483–1496, 1990.

Cooley, R. L., Some new procedures for numerical solution of variably saturated flow problems, *Water Resour. Res.*, *19*(5), 1271–1285, 1983.

Dennis, J. E., and J. J. Moré, Quasi-Newton methods, motivation and theory, *SIAM Rev.*, *19*(1), 46–89, 1977.

Faust, C. R., Transport of immiscible fluids within and below the unsaturated zone: A numerical model, *Water Resour. Res.*, *21*(4), 587–596, 1985.

Freund, R. W., A transpose-free quasi-minimal residual algorithm for non-Hermitian linear systems, *SIAM J. Sci. Comput.*, *14*, 470–482, 1993.

Frind, E. O., and M. J. Verge, Three-dimensional modeling of groundwater flow systems, *Water Resour. Res.*, *14*(5), 844–856, 1978.

Gambolati, G., and A. Perdon, Conjugate gradients in subsurface flow and land subsidence modeling, in *Fundamentals of Transport Phenomena in Porous Media*, edited by J. Bear and M. Y. Corapcioglu, pp. 953–984, Martinus Nijhoff, Dordrecht, Netherlands, 1984.

Hills, R. G., I. Porro, D. B. Hudson, and P. J. Wierenga, Modeling one-dimensional infiltration into very dry soils, 1, Model development and evaluation, *Water Resour. Res.*, *25*(6), 1259–1270, 1989.

Huyakorn, P. S., and G. F. Pinder, *Computational Methods in Subsurface Flow*, Academic, San Diego, Calif., 1983.

Huyakorn, P. S., S. D. Thomas, and B. M. Thompson, Techniques for making finite elements competitive in modeling flow in variably saturated porous media, *Water Resour. Res.*, *20*(8), 1099–1115, 1984.

Huyakorn, P. S., J. W. Mercer, and D. S. Ward, Finite element matrix and mass balance computational schemes for transport in variably saturated porous media, *Water Resour. Res.*, *21*(3), 346–358, 1985.

Huyakorn, P. S., E. P. Springer, V. Guvanasen, and T. D. Wadsworth, A three-dimensional finite-element model for simulating water flow in variably saturated porous media, *Water Resour. Res.*, *22*(13), 1790–1808, 1986.

Kershaw, D. S., The incomplete Cholesky–conjugate gradient method for the iterative solution of systems of linear equations, *J. Comput. Phys.*, *26*, 43–65, 1978.

Kuiper, L. K., A comparison of iterative methods as applied to the solution of the nonlinear three-dimensional groundwater flow equation, *SIAM J. Sci. Stat. Comput.*, *8*, 521–528, 1987.

Matthies, H., and G. Strang, The solution of nonlinear finite element equations, *Int. J. Numer. Methods Eng.*, *14*, 1613–1626, 1979.

Neuman, S. P., Saturated-unsaturated seepage by finite elements, *J. Hydraul. Div. Am. Soc. Civ. Eng.*, *99*(HY12), 2233–2250, 1973.

Ortega, J. M., and W. C. Rheinboldt, *Iterative Solution of Nonlinear Equations in Several Variables*, Academic, San Diego, Calif., 1970.

Paniconi, C., Hydrologic processes in variably saturated porous media: Analysis of numerical methods for solving the nonlinear Richards equation, and application to catchment scale simulations, Ph.D. dissertation, Dep. of Civ. Eng. and Oper. Res., Princeton Univ., Princeton, N. J., 1991.

Paniconi, C., and E. F. Wood, A detailed model for simulation of catchment scale subsurface hydrologic processes, *Water Resour. Res.*, *29*(6), 1601–1620, 1993.

Paniconi, C., A. A. Aldama, and E. F. Wood, Numerical evaluation of iterative and noniterative methods for the solution of the nonlinear Richards equation, *Water Resour. Res.*, *27*(6), 1147–1163, 1991.

Philip, J. R., Theory of infiltration, *Adv. Hydrosci.*, *5*, 215–296, 1969.

Pini, G., G. Gambolati, and G. Galeati, 3-D finite element transport models by upwind preconditioned conjugate gradients, *Adv. Water Resour.*, *12*, 54–58, 1989.

Pullan, A. J., The quasi-linear approximation for unsaturated porous media flow, *Water Resour. Res.*, *26*(6), 1219–1234, 1990.

Putti, M., and C. Paniconi, Evaluation of the Picard and Newton iteration schemes for three-dimensional unsaturated flow, in *Proceedings of the IX International Conference on Computational Methods in Water Resources*, vol. 1, *Numerical Methods in Water Resources*, edited by T. F. Russell, R. E. Ewing, C. A. Brebbia, W. G. Gray, and G. F. Pinder, pp. 529–536, Computational Mechanics Publications, Billerica, Mass., 1992.

Putti, M., W. A. Mulder, and W. W.-G. Yeh, A time-accurate multigrid algorithm for the solution of the transport equations, in *Computational Methods in Surface Hydrology: Proceedings of the VIII International Conference on Computational Methods in Water Resources*, edited by G. Gambolati, A. Rinaldo, C. A. Brebbia, W. G. Gray, and G. F. Pinder, pp. 441–447, Computational Mechanics Publications, Billerica, Mass., 1990.

Ross, P. J., Efficient numerical methods for infiltration using Richards' equation, *Water Resour. Res.*, *26*(2), 279–290, 1990.

Stauffer, F., Numerical simulation of infiltration into porous media and response of the water table, in *Proceedings of the Fourth International Conference on Finite Elements in Water Resources*, edited by K. P. Holz, U. Meissner, W. Zielke, C. A. Brebbia, G. F. Pinder, and W. G. Gray, pp. 10.73–10.82, Springer-Verlag, New York, 1982.

Stoer, J., and R. Bulirsch, *Introduction to Numerical Analysis*, Springer-Verlag, New York, 1980.

van der Vorst, H., Bi-CGSTAB: A fast and smoothly converging variant of BI-CG for the solution of nonsymmetric linear systems, *SIAM J. Sci. Stat. Comput.*, *13*, 631–644, 1992.

van Genuchten, M. T., and D. R. Nielsen, On describing and predicting the hydraulic properties of unsaturated soils, *Ann. Geophys.*, *3*(5), 615–628, 1985.

C. Paniconi, CRS4, Via Nazario Sauro 10, 09123 Cagliari, Italy.
M. Putti, Dipartimento di Metodi e Modelli Matematici per le Scienze Applicate, Università di Padova, Via Belzoni 7, 35131 Padova, Italy.

(Received November 3, 1993; revised April 1, 1994; accepted August 9, 1994.)